TECHNICAL REPORT 2016
April 2013

Convergence of the Quasi-static Antenna Design Algorithm

T. O. Jones III

SSC Pacific
San Diego, CA 92152-5001

TECHNICAL REPORT 2016
April 2013

Convergence of the Quasi-static Antenna Design Algorithm

T. O. Jones III

SSC Pacific
San Diego, CA 92152-5001

SSC Pacific
San Diego, California 92152-5001

J.J. Beel, CAPT, USN
Commanding Officer

C. A. Keeney
Executive Director

ADMINISTRATIVE INFORMATION

This report was prepared for the by the ISR/IO Department (Code 56), SPAWAR Systems Center Pacific, San Diego, CA.

Released by
M. D. Osburn, Head
Electromagnetics Technology
Branch

Under authority of
J. McGee, Head
SoS & Platform Design
Division

MatLab® is a registered trademark of The Math Works.

SB

EXECUTIVE SUMMARY

The quasi-static antenna design algorithm uses multipole basis function to model the general thick top load. A sequence of solutions converge in shape and Q. The absolute minimum Q-factor, 1.825, is obtained for a thick disk top load enclosed by a sphere. This is significantly smaller than the thin disk top load Q-factor 2.349 and previously derived thick-disk Q-factor 2.078. An analytic potential is derived for each multipole basis function. The capacitance and effective height is calculated from the potentials on the enclosing sphere. The impedance is computed with Computer Simulation Technology (CST) Microwave Studio. The impedance data is numerically fit to a dipole eigenmode equivalent circuit. The radiation resistance does not fit the expected ω^2 frequency dependence (effective height).

The error is an ω^4 term that is explained by a capacitor approximated for the octupole eigenmode equivalent circuit. The quasi-static antenna design algorithm predicts the DC capacitance and the dipole eigenmode effective height. The octupole eigenmode increases the radiation resistance. The Q-factor, 1.77, is lower than expected. These results are compared to the spherical cap top load. The existence of an ω^4 limits the accuracy of the theoretical limits in the Q values for antennas.

CONTENTS

Figures

Tables

1. INTRODUCTION

Electrically small antennas are common to portable electronics devices, personal digital assistants (PDAs), cell phones, etc. These antennas are small compared to wavelength or electrical small antennas. Designing electrically small antennas is an art; they normally have a low radiation resistance, a large reactance, and a small bandwidth. Additional matching components are required to eliminate the reactance and increase the resistance. The objective of this work is to increase the radiation resistance, decrease reactance, and maximize the bandwidth. The quasi-static antenna design algorithm is more science than art.

L. J. Chu [1] derived a lower limit for the Q, for electrically small antennas. Chu's Q calculation is based on the radiated energy and the stored energy outside a sphere enclosing the antenna; the energy inside the sphere is assumed to be zero. H. L. Thal [2] refined this limit by assuming the antenna current is limited to the surface of the enclosing surface. The folded spherical helix design by S. R. Best [3] meets Thal's limit for TM_{10}. M. Gustafsson, C. Sohl, and G. Kristensson [4] derived a Q limit based on the optical theorem. A. D. Yaghjian and H. Stuart [5] derived a more restrictive limit on Q.

The energy inside the sphere limits the antenna performance. The thin disk-loaded monopole is a leaky capacitor with a large amount of stored energy inside the sphere. The electric field under the disk is larger than the field above the disk. The quasi-static antenna design algorithm [6, 7] analytically computed a thick disk-loaded dipole. The thick disk-loaded dipole reduces stored energy and Q by filling some of the spherical volume with conductor. The electric field under the top load is still larger than the field above the top load. This paper shows how to reduce the electric field under the top load and increases the radiation resistance of the antenna [8]. The antenna shape shifts to eliminate the gap (and the energy) between the top of the antenna and the enclosing sphere. The stored energy inside the enclosing sphere is limited to the region between the antenna and the ground.

Electrically small antennas have electric fields much larger than the magnetic fields below the antenna resonance. The Asymptotic Conical Dipole (ACD) [9, 10, 11] was the first antenna design with quasi-static methods. In electrostatics, a perfect conductor is the same as an equipotential surface. A line of constant charge on the z-axis, with an image, will generate the ACD antenna design. Each ACD antenna has a different height. The quasi-static antenna design algorithm [7] fixes the antenna height to a constant a and the length of the line charge κa is varied; the antenna fits within an enclosing sphere with a radius a. The parameter κ is a dimensionless. The Q is calculated from

$$Q = \frac{1}{\omega C R_{Rad}}, \tag{1}$$

where R_{Rad} is radiation resistance, C is capacitance, and ω is angular frequency. The quantities R_{Rad} and C are functions of κ. The radiation resistance is calculated from the effective height. The capacitance is calculated from the charge on the antenna arm and the maximum potential on the spherical enclosing surface with a radius a.

The above equation for Q is valid below resonance and it gives only the first term in Chu's equation:

$$Q > \frac{1}{(ka)^3} + \frac{1}{ka}, \tag{2}$$

where $k = 2\pi / \lambda$ and a is the radius of the enclosing sphere. The ACD design is extended by adding a disk-shaped charge distribution as a load on the line charge [7]. A disk in free space is used as the charge distribution. The disk charge distribution is symmetric. The electric fields between the disks and image will be larger than the electric fields above the disk. There is no requirement for the disk charge distribution to be symmetric. Adding a dipole moment moves the charge from the bottom of the disk to the top of the disk. This reduces the electric field between the disks. A series of multipole charge distributions can be added to the disk to model the general charge distribution on the disk.

Sections 2 and 3 are not needed to understand the results given in Sections 4 and 5. Section 2 shows how the potential and top load capacitance is computed from electrostatic solutions in oblate spheroidal coordinates. Each solution represents a unique multipole moment with an unique potential. Only the rotationally symmetric top-load multipole modes will be used in this model. The n^{th} multipole falls off as $\frac{1}{r^{n+1}}$ in the far field. The potential for the dipole multipole term and high odd moments add in the far field. The monopole and higher even moments cancel in the far fields. All of the multipole make a unique and diminishing contribution to the near fields.

The perfect conductor boundary condition, $E_{\|} = 0,$ requires the charge distribution to be enclosed by the antenna surface. Only a subset of the charge distributions satisfies this boundary condition. The multipole moments have negative potentials, which can cause the equipotential surface to terminate on the disk or feed wire. This requires an additional step in the solution process; the equipotential surface is sampled to verify that the charge is enclosed by the equipotential surface. The final solution must be verified with a detailed calculation of the antenna shape. In Section 3, the effective height is calculated. The effective height calculation with dipole moment top load is non-trivial. The effective height cannot be calculated with the conventional formula [8]. The effective height is calculated indirectly from the potential on the enclosing sphere.

In Section 4, a sequence of multipole basis functions are used to design minimum Q antennas. The antenna designs appear to converge in both shape and $Q.$ The final antenna design fills the top of the sphere; the area under the antenna is the only region with electric fields that contributes to stored energy inside the enclosing sphere. The electric field on the surface of the antenna is plotted. The electric field under the antenna is reduced by adding multipole moments. The final antenna also has an almost horizontal lower surface.

In Section 5, Computer Simulation Technology (CST) Microwave Studio is used to calculate the impedance and Q for a 1-m high antenna with a 1-cm-diameter hollow feed line. The impedance is calculated with a sequence of energy-based adaptive iterations. L. J. Chu [1]; H. D. Foltz, J. S. McLean, and L. Bodner [12]; and H. R. Stuart [13] used a series L, C with a resistor, R_0, parallel to the inductor to model both the reactance and ω^2 dependence radiation resistance. The model represents the dipole eigenmode. The least squares fit to the CST impedance is a good fit to the reactance. The radiation resistance has an obvious error. The radiation resistance has an ω^2 and ω^4 frequency-dependence terms; the coefficients are calculated with a least square fit. The ω^2

contribution gives the same effective height as the quasi-static antenna design algorithm. The ω^4 frequency-dependence term is the source of the error in the circuit model.

The next eigenmode, the octupole, is a circuit connected in parallel with the first eigenmode model [13]. The octupole (and higher) equivalent circuits reduces to a capacitor at low frequencies. This capacitance combined with dipole eigenmode circuit gives an anti-resonance. The dipole and octupole eigenmode currents interfere with each other to create a high impedance at anti-resonance. The anti-resonance does not have a deep physical meaning. The combined dipole eigenmode model and higher eigenmode capacitance significantly improve the numerical fit to the CST impedance data. The capacitance value was calculated from the anti-resonance frequency; the other circuit elements L, C, and R_0, were unchanged. The improved fit to the radiation resistance data is attributed to a ω^4 frequency-dependant term introduced by the parallel capacitance. The simple equivalent circuit for the octupole does include any radiation resistance. The higher radiation resistance reduces the Q-factor below the value predicted by the quasi-static antenna design algorithm. The extra capacitance introduced by the feed line is estimated. The quasi-static antenna design algorithm gives both the DC capacitance and the ω^2 dipole radiation resistance.

In Section 6, CST is also used to calculate the impedance of the spherical top-loaded monopole. The same feed wire was used for the 1-m spherical top-loaded monopole. The data is fit to the same dipole eigenmode with a capacitor approximation of higher eigenmodes. The capacitance of the top-load is larger than the above design. The effective height is smaller. The Q-factor is lower than the result obtained by A. R. Lopez [14]. Electrostatic data is not available to compare to the circuit results.

Section 7 is the conclusion. The quasi-static antenna design algorithm gives a solution very close to the spherical capped monopole (the top-loaded design with the lowest Q). The algorithm does not model all possible antenna shapes. The algorithm does not allow the bottom surface of the antenna to be above the source charge on the disk. A thick spherical cap top-load antenna could have a lower Q. The quasi-static antenna design algorithm produces a very good antenna design with modest effort. Other designs can be computed with a significantly higher radiation resistance and a slightly larger Q. The algorithm can be adapted to other enclosing surfaces.

2. CAPACITANCE FOR THE OBLATE SPHEROIDAL ANTENNA

The detailed discussion of the algorithm is given in Reference [7]. This discussion is the more general case. The capacitance of the general thick top load is calculated from the potential on enclosing surface $(q = CV)$. The potential is calculated from an analytic solution to the electrostatic equations. The top of the hollow feed line has a height κa and $(1-\tau)q$ charge; the potential [15, 16] is

$$\Phi^{ACD}(\rho, z) = \frac{(1-\tau)q}{4\pi\varepsilon_0 \kappa a} \ln\left(\frac{(1+\delta_m)(1-\delta_i)}{(1-\delta_m)(1+\delta_i)}\right), \tag{3}$$

where $\delta_m = \frac{\kappa a}{R_f + R_t}$ is for the monopole, $\delta_i = \frac{\kappa a}{R_f + R_b}$ is for the image monopole, $R_t = \sqrt{(z-\kappa a)^2 + \rho^2}$ is the distance from ρ, z to the top of the monopole, $R_f = \sqrt{z^2 + \rho^2}$ is the distance from ρ, z to the feed point, and $R_b = \sqrt{(z+\kappa a)^2 + \rho^2}$ is the distance from ρ, z to the bottom of the image monopole. The parameter τ is the fraction of the total charge q on the antenna top load. The superscript indicates an ACD stem. The parameter κ is dimensionless and $0 < \kappa < 1$.

The disk also has the height κa, a disk radius of αa, and a net charge τq where the parameter α is dimensionless and has the range of values $0 < \alpha < \sqrt{1-\kappa^2}$. G. Arfken [17, pp. 599-601 and 596] gives the general solution to potential on the disk $\nabla^2 \Phi(u, v, \phi) = 0$. The potential on the disk is a linear combination of multipole moments $K_n(u) P_n^m(\cos v) e^{im\phi}$ where v and u are defined by the oblate spheroidal coordinate system:

$$z = \alpha a \sinh(u) \cos(v), \tag{4}$$

$$x = \alpha a \cosh(u) \sin(v) \cos(\phi), \tag{5}$$

$$y = \alpha a \cosh(u) \sin(v) \sin(\phi), \tag{6}$$

where the αa is the disk radius.. The antenna problem will be simplified by assuming rotational symmetry where $\rho = \alpha a \cosh(u) \cos(v)$:

$$\Phi(u, v, \phi) = \sum_{n=0}^{\infty} \sum_{m=0}^{m=n} \frac{b_{nm}}{\alpha^n} K_n(u) P_n^m(\cos v) e^{im\phi}, \tag{7}$$

The rotational symmetry in ϕ requires $b_{mn} = 0$ for $m > 0$ and the associated Legendre Polynomials reduce to Legendre Polynomials, $P_n^0(\cos v) = P_n(\cos v)$. The $1/\alpha^n$ is added for numerical convenience. The $K_n(u)$ functions are as follows:

$$K_0(\sinh u) = \operatorname{arccot}(\sinh u), \tag{8}$$

$$K_1(\sinh u) = 1 - \sinh(u)\operatorname{arccot}(\sinh(u)), \tag{9}$$

$$K_2(\sinh u) = \left[(3\sinh^2(u).+1)\operatorname{arccot}(\sinh(u)) - 3\sinh(u)\right]/2, \tag{10}$$

and

$$K_3(\sinh u) = -\left(\frac{5}{2}\sinh^3(u) + \frac{3}{2}\sinh(u)\right)\operatorname{arccot}(\sinh(u)) + \frac{5}{3}\left(\frac{3}{2}\sinh^2(u) + \frac{1}{2}\right) - \frac{1}{6}. \tag{11}$$

The general case is

$$K_n(\xi) = \left(-i^{n+1}\right)Q_n(i\xi), \tag{12}$$

where

$$Q_n(i\xi) = (-i)P_n(i\xi)\operatorname{arccot}(\xi) - \frac{(2n-1)}{n}P_{n-1}(i\xi) - \frac{(2n-5)}{3(n-1)}P_{n-3}(i\xi) - \ldots \tag{13}$$

The function K_n at large distance is calculated by expanding $a\cot(snh(u)) = a\tan\left(1/\sinh(u)\right)$ in a power series of $\frac{1}{\sinh(u)}$. After simplifying, the leading term is

$$K_0 \approx \frac{1}{\sinh(u)} \quad \text{for} \quad u \gg 2, \tag{14}$$

$$K_1 \approx \frac{2}{3}\frac{1}{\sinh^2(u)} \quad \text{for} \quad u >> 2, \tag{15}$$

$$K_2 \approx \frac{2}{15}\frac{1}{\sinh^3(u)} \quad \text{for} \quad u \gg 2, \tag{16}$$

and

$$K_3 \approx \frac{2}{35}\frac{1}{\sinh^4(u)} \quad \text{for} \quad u \gg 2 \tag{17}$$

since $\alpha a \sinh(u) = z$, the above equations reduce to $\frac{\alpha a}{z}$, $\frac{2}{3}\left(\frac{\alpha a}{z}\right)^2$, $\frac{2}{15}\left(\frac{\alpha a}{z}\right)^3$, and $\frac{2}{35}\left(\frac{\alpha a}{z}\right)^4$. This is the expected multipole expansion of the field on the z-axis. Figure 1 plots K_n as a function of $\sinh(u)$; this shows the $\frac{1}{z^{n+1}}$ dependence. The factor $\frac{1}{\alpha^n}$ is included in Equation 7 to eliminate the α^n dependence in the far field. The value of $b_{00} = \frac{\tau q}{4\pi\varepsilon_0 a}$ is calculated from the solution of the disk in free space $V(u) = \frac{\tau q}{4\pi\varepsilon_0 \alpha a}\operatorname{arccot}(\sinh u)$, where τq is the net charge on the disk. The only restrictions placed on the values of b_{nm} is the charge distribution must be enclosed within an equipotential surface.

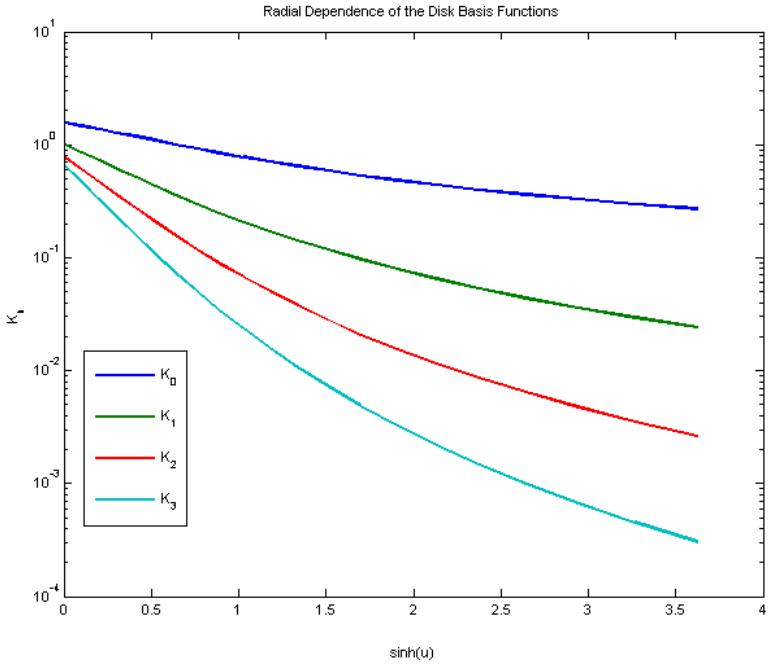

Figure 1. First four top-load radial multipole basis function.

The combined potential is

$$\Phi(z,\rho) = \Phi^{ACD}(\rho,z) + \Phi^{TopDisk}(u_t,v_t) - \Phi^{BotDisk}(u_b,v_b), \tag{18}$$

where the variables u_t, v_t, and u_b, v_b are defined from

$$z - \kappa a = \alpha a \sinh(u_t)\cos(v_t), \tag{19}$$

$$\rho = \alpha a \cosh(u_t)\sin(v_t), \tag{20}$$

$$z + \kappa a = \alpha a \sinh(u_b)\cos(v_b), \tag{21}$$

$$\rho = \alpha a \cosh(u_b)\sin(v_b). \tag{22}$$

The capacitance is calculated from the maximum value of $\Phi(z,\rho)$ on the sphere $z = a\cos\theta$ and $\rho = a\sin\theta$:

$$\Phi_{Max} = \max\left(\Phi(a\cos\theta, a\sin\theta)\right) \text{ where } 0 \le \theta \le \pi/2 \tag{23}$$

and

$$C = \frac{q}{\Phi_{Max}}. \tag{24}$$

In the above coordinate systems, $v_t = 0$ and $v_b = 0$ are defined in the $+z$ direction. The charge distribution that generates the term $\Phi^{BotDisk}(u_b, v_b)$ is the mirror image of the charge distribution for $\Phi^{TopDisk}(u_t, v_t)$:

$$\Phi^{TopDisk}(u_t, v_t) = \sum_{n=0}^{\infty} \frac{b_n}{\alpha^n} K_n(u_t) P_n(\cos v_t) \tag{25}$$

and

$$\Phi^{BotDisk}(u_b, v_b) = \sum_{n=0}^{\infty} (-1)^n \frac{b_n}{\alpha^n} K_n(u_b) P_n(\cos v_b). \tag{26}$$

The sign on $\frac{b_n}{\alpha^n} K_n(u_b) P_n(\cos v_b)$ follows from $P_n(\cos v_b)$, being even or odd relative to $v = \pi/2$. The dipole term is the simplest example to understand: $K_1(u_t) P_1(\cos v_t)$ has positive charge on the top of the disk and $K_1(u_b) P_1(\cos v_b)$ has positive charge on the top of the image disk (top is +z direction for both disks). Both terms have a negative charge on the bottom of the disk and image disk. The combined terms

$$K_1(u_t) P_1(\cos v_t) + K_1(u_b) P_1(\cos v_b) \tag{27}$$

are odd about $z = 0$. For the case $b_1 > 0$, the dipole moment of the antenna is increased and the electric field under the antenna is decreased (with the other parameters unchanged). In the general case, when n is odd, the terms

$$K_n(u_t) P_n(\cos v_t) + K_n(u_b) P_n(\cos v_b) \text{ for odd } n \tag{28}$$

increase the n^{th} moment. When n is even, the terms

$$K_n(u_t) P_n(\cos v_t) - K_n(u_b) P_n(\cos v_b) \text{ for even } n \tag{29}$$

subtract in the far field the first contributing far-field moment is the $(n+1)^{th}$ moment. Each term has a unique contribution to the electric field under the antenna.

The next step is to compute the radiation resistance.

3. GENERAL CALCULATION OF RADIATION RESISTANCE

The effective height for a rotationally symmetric charge distribution is

$$h_{Eff} = \frac{1}{q_{Net}} \int_{z=0}^{z=a} \int_{\rho=0}^{\rho=\sqrt{a^2-z^2}} zq(\rho,z) 2\pi\rho d\rho dz. \tag{30}$$

From a previous paper [6, 7], this simplifies to

$$h_{Eff} = \frac{\kappa a}{2}(1-\tau) + \kappa a \tau. \tag{31}$$

How to apply the above effective height calculation to the dipole term $K_1(u)P_1(\cos v)$ is not obvious. The $K_1(u)P_1(\cos v)$ term is discontinuous at $u = 0$. The function is odd about $v = \pi/2$ or $K_1(0)P_1(\cos v) = -K_1(0)P_1(\cos(\pi - v))$. The dipole term would give zero for a thin disk with no net charge. The above equation is only valid for even potentials on the disk (monopoles, quadrupoles, etc.).

To derive the general case, the dipole moment used as the starting point is

$$\mathbf{p}_z = \int_{z=-a}^{z=a} \int_{\rho=0}^{\rho=\sqrt{a^2-z^2}} zq(\rho,z) 2\pi\rho d\rho dz. \tag{32}$$

The potential outside (and on) the sphere can be represented as a sum of spherical harmonics:

$$\Phi(r,\theta) = \sum_{n=1}^{\infty} \beta_{n0} \left(\frac{a}{r}\right)^{n+1} P_n(\cos\theta) \ \ for\ r \geq a, \tag{33}$$

where $p_z = \beta_{10} a^2$ and $r = \sqrt{z^2 + p^2}$ with all of the charge enclosed in a sphere of radius a. The dipole moment is computed from the potentials,

$$\mathbf{p}_z = \frac{3}{2} a^2 \int_{\theta=0}^{\theta=\pi} \Phi(a,\theta) P_1(\cos\theta) \sin\theta d\theta. \tag{34}$$

This term is independent of the charge distribution. The effective height is

$$h_{Eff} = \frac{1}{2q_{Net}} \mathbf{p}_z. \tag{35}$$

4. GENERAL OBLATE SPHEROIDAL ANTENNA

In the calculation for the thin disk-loaded monopole, the feed line is neglected. The capacitance calculation assumes all of the charge is on the top load disk. This model includes a hollow feed line. The Matlab® calculation of the Oblate Spheroidal Antenna (OSA) assumes that 99% of the charge is on the top load and a token 1% of the charge is on the feed line: $\tau = 0.99$ and $(1-\tau) = 0.01$. As shown in Figure 2, the antenna designs appear to converge in shape and Q.

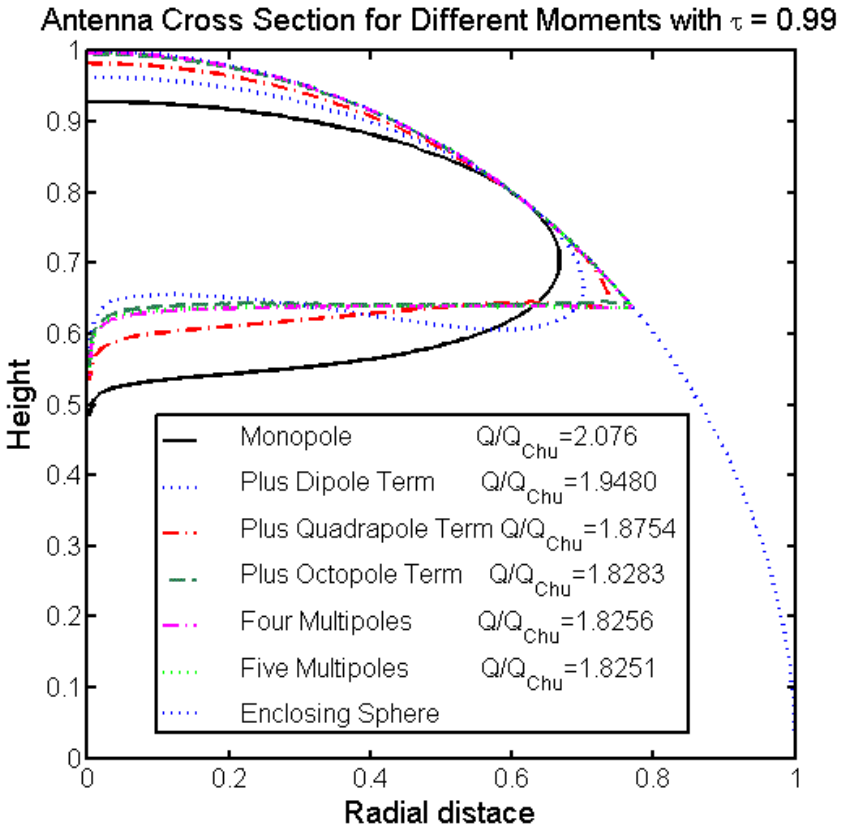

Figure 2. A sequence of antenna designs with one to five load multipoles.

Figure 3 shows a detailed plot of the antenna surface near the sphere. Spherical coordinates $r = \sqrt{z^2 + \rho^2}$ are used for the vertical axis and $\theta = \arcsin(\rho / r)$ is used for the horizontal axis. As basis functions are added the antenna design, the shape approaches the surface of the enclosing sphere. Figure 3 shows that adding extra multipole moments has a diminishing impact on the Q-factor. The multipole moments fall off as $1/r^{n+1}$; they have diminishing impact on the electric field outside the sphere and under the antenna. The electric field is calculated from the potential and plotted in Figure 4.

The vertical scale is electric field magnitude plotted as a function of distance along the surface measured from the top of the antenna, $z = 1$ and $\rho = 0$. The spike in the electric field is at the transition from almost spherical surface to the underside of the antenna. For the solution with five multipoles, this transition is very sharp. The electric field under the antenna is reduced by the dipole

moment term. Figure 4 shows that the position of the spike moves to the right as multipoles are added. This increases the surface area of the top surface of the antenna and the total charge on the top of the antenna.

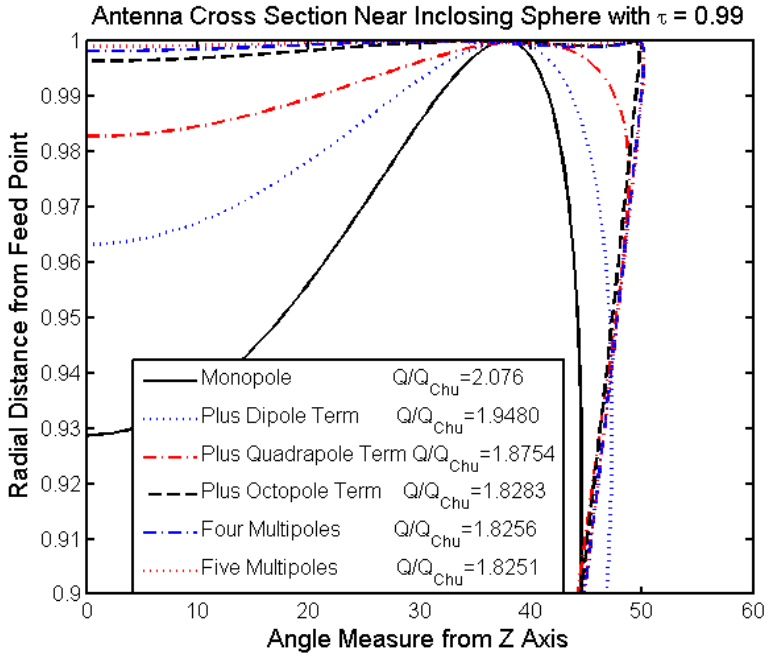

Figure 3. The antenna shape near the enclosing surface.

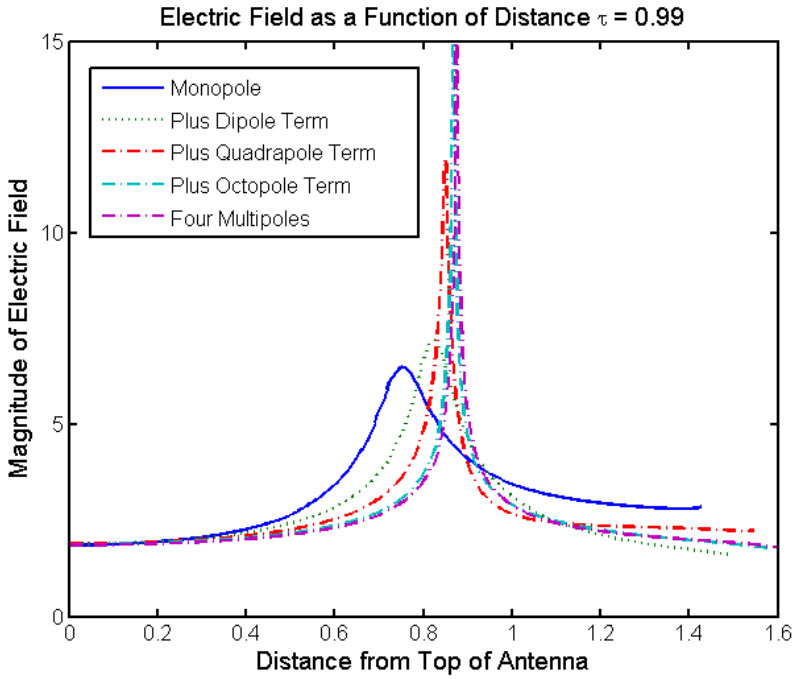

Figure 4. Electric field calculated as a function of distance from the antenna top.

5. SECTION CST MODEL OF OBLATE SPHERICAL ANTENNA

Computer Simulation Technology (CST) Microwave Studio was used to model the antenna. An accurate model for the energy is critical for Q calculations. CST includes an energy-based adaptive meshing that increases the mesh resolution in areas of high-energy density. A sequence of adaptive meshing models were run to refine the starting mesh for the next model[1]. A 4.3-ohm cylindrically edge port was used at the hollow feed point and the excitation frequency range was from 15 to 25 MHz; this reduces the energy reflected at the input to the antenna[2]. The hollow feed line was modeled independently to determine the required meshing. The convergence in the solutions is evaluated by looking at the largest difference between previous and current S_{11}. In the final run, this difference is 3.4e-4. The process was time consuming, but it eliminated the risk of using too fine a mesh and introducing numerical errors in the solution.

The antenna capacitance and effective height can be extracted from the CST impedance data ($\rho \le 0.5$) with a MatLab program. The MatLab program calculated the least square best fit to Stuart's eigenmode impedance circuit model, Figure 5 and Table 1. The fit to the reactance was very good but the radiation resistance has a large error. An additional octupole eigenmode can be modeled at low frequencies as a parallel capacitor $C_{OSA\,OP+}$ where the subscript indicates octupole plus higher order eigenmodes (the inductors short the other circuit elements at low frequencies). This extra capacitance adds an antiresonance to the single eigenmode impedance. Another CST model was run to calculate the antiresonance frequency, 90.916 MHz. The value of $C_{OSA\,OP+}$ was calculated based on this frequency and the previously calculated values of R_0, C, and L.

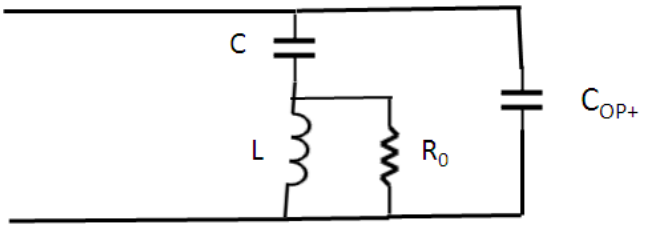

Figure 5. The equivalent circuit for the first and second eigenmode approximation.

Figure 6 shows the CST impedance and the two eigenmodes circuit approximation. The difference is so small it is plotted in Figure 7. The circuit parameters are in Table 1. The C_{DC}^{CST} capacitance is

$$C_{DC}^{CST} = C_{OSA}^{CST} + C_{OSA\,OP+} = 95.032. \tag{36}$$

[1]Shrikrishna Hegde at Sonnent Software provided insight into energy adaptation and meshing.

[2]James Whillhite at Sonnent Software suggested matching the a source resistance to the antenna and using a narrow frequency range to maximize the energy delivered to the antenna.

Table 1. Least square best fit to Stuart's eigenmode impedance circuit model.

Parameters	Eigenmode 1	Eigenmode 1 & 2	QSADA
C_{OSA}	90.2683 pF	90.2683 pF	90.364 pF
L_{OSA}	0.6758598 μH	0.6758598 μH	N/A
$R_{0\,OSA}$	1.96632 KΩ	1.96632 KΩ	N/A
f_{RES}	20.39706 MHz	20.39705 MHz	N/A
h_{Eff}	N/A	0.7063	0.7108
$C_{OSA\,OP+}$	N/A	4.7638 pF	N/A
$f_{Antiresonance}$	N/A	90.916 MHz	N/A
Q-factor	N/A	1.77	1.82

The impact of the finite diameter feed line can be estimated. The current on the feed line is almost constant; almost all of the charge flows onto the top load. A reasonable approximation for the charge distribution on the feed line is a triangular distribution. The net charge on the feed line is 1/2 the monopole charge (constant charge distribution for electrical small monopole). The capacitance of a monopole 0.587-m high is 6.2 pF. The feed-line capacitance is about 3.1 pF. The quasi-static antenna design algorithm (QSADA) assumes 1% of the total charge is on the feed line or the feed line capacitance is 0.9 pF $\left(=0.01*90.364\,\text{pF}\right)$. This difference is $C^{Stem}=2.2$ pF. The difference between the two calculations is about 2.4 pF or about 2.6%:

$$C_{DC}^{QS}=C_{OSA}^{QS}+C^{Stem}=92.6. \tag{37}$$

The resistance has two components, ω^2 and ω^4 terms

$$R_{OSA}=b_1\left(\omega/\omega_r\right)^2+b_2\left(\omega/\omega_r\right)^4, \tag{38}$$

where ω_r is the angular resonant frequency, $b_1=3.6465$ and $b_2=0.4575.$ Figure 8 shows the curve fit. The effective height in Table 1 is calculated from the ω^2 term in the radiation resistance; it agrees with the quasi-static antenna design algorithm. The radiation resistance circuit element is not included in the octupole eigenmode circuit model. The ω^4 term is caused by a circulating current in the parallel CL circuit. This current is higher than the current in the dipole eigenmode equivalent circuit. The antenna Q will be lower than predicted by the quasi-static antenna design algorithm.

The Q, Figure 9, was calculated using the Yaghijian and Best [18] result:

$$Q=\frac{\omega}{2R}\sqrt{\left(\frac{dR}{d\omega}\right)^2+\left(\frac{|X|}{\omega}+\frac{dX}{d\omega}\right)^2}. \tag{39}$$

Figure 10 shows the $Q(ka)^3$ "Q-factor" for the antenna that was calculated from a two-eigenmode circuit approximation. The Q curves are calculated numerically from the fit data. The minimum Q-factor is 1.77.

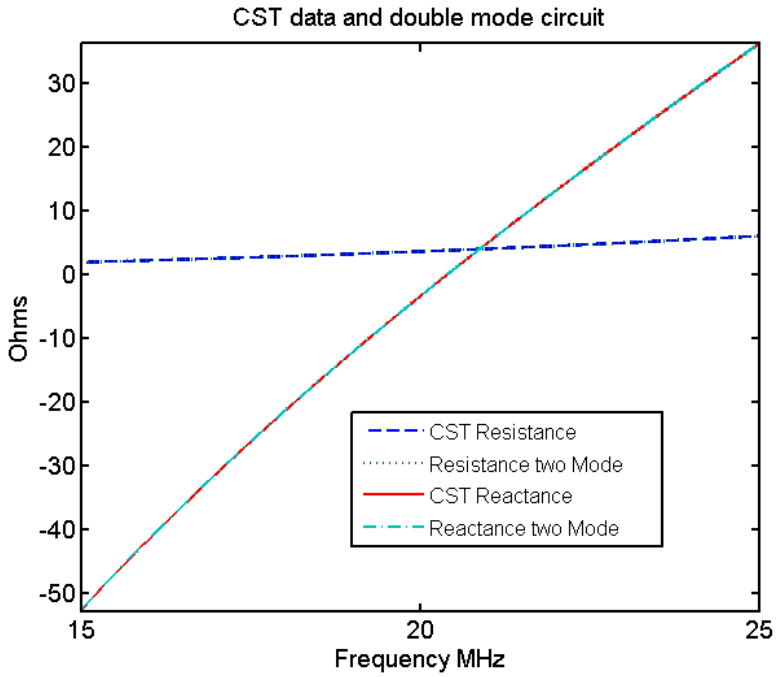

Figure 6. CST data and equivalent circuit model.

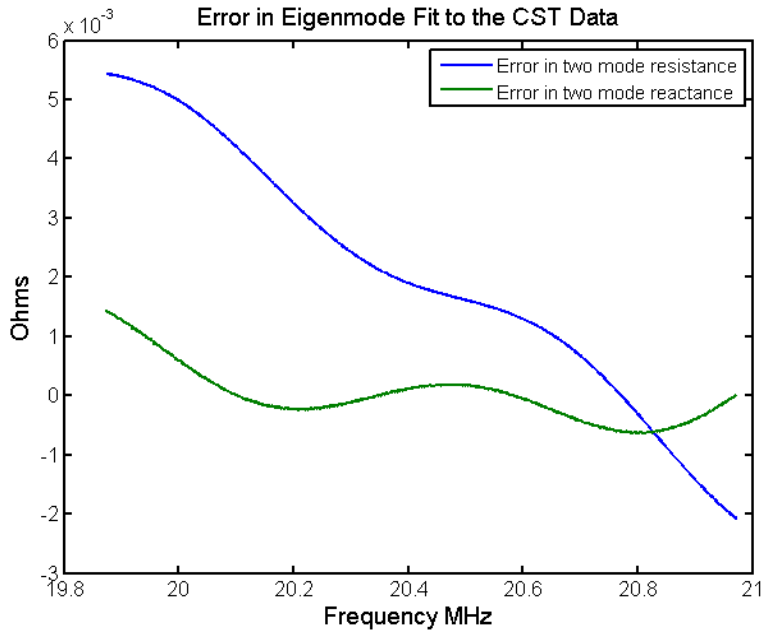

Figure 7. Error in eigenmode model. Typical error is a few milliohms.

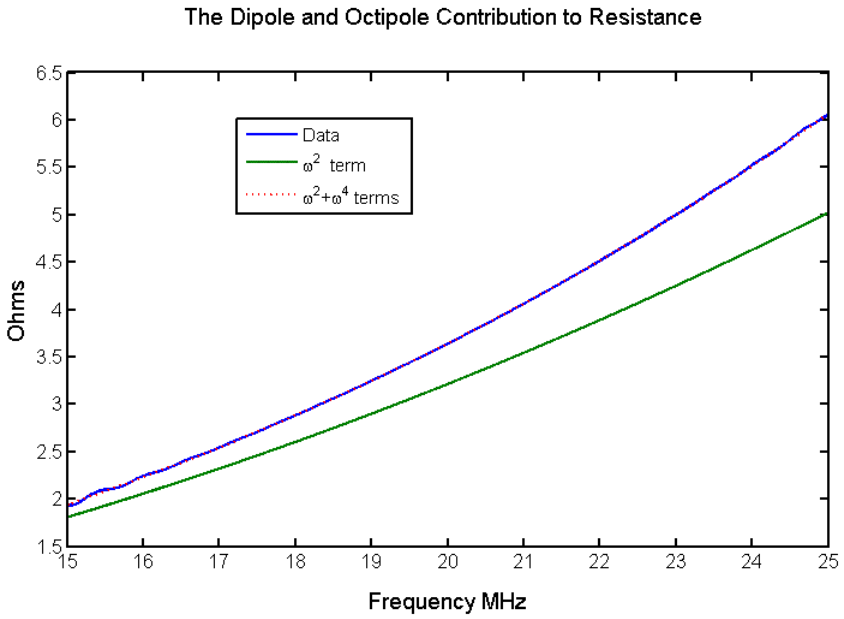

Figure 8. ω^2 and ω^4 contribution to resistance.

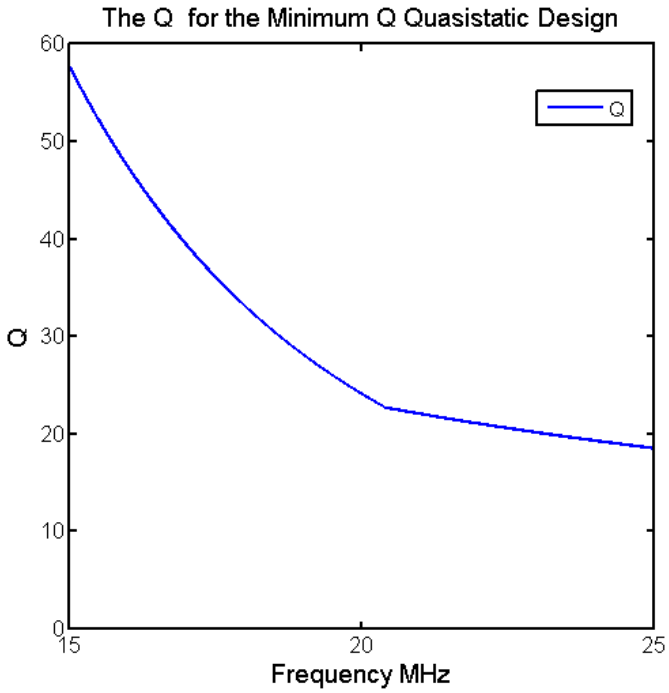

Figure 9. Q for the minimum Q OSA design.

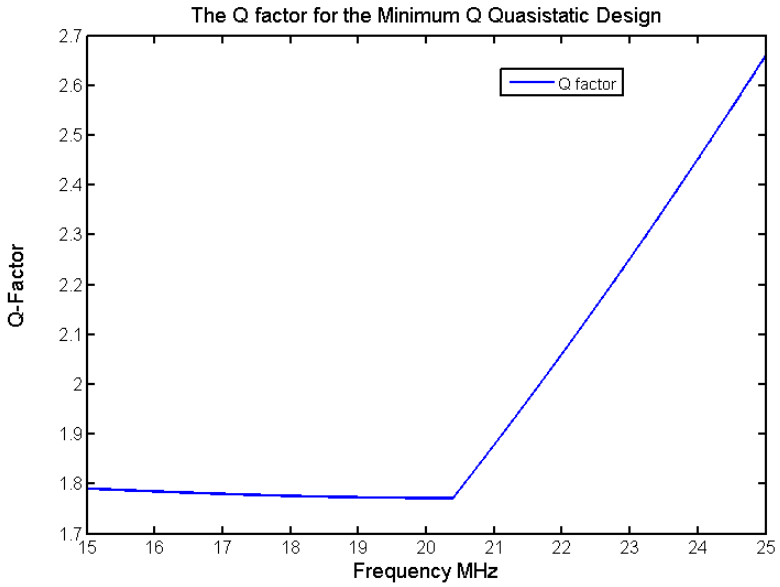

Figure 10. Q-factor for the minimum Q OSA design.

6. CST MODEL OF A SPHERICAL TOP LOAD

The same method was used to model a spherical top load. The spherical top load is a much harder problem. The edge of the spherical top load will have a much higher field than the above solution; this requires a higher resolution near the edge of the spherical top load. If the edge thickness was set too small, CST will not accurately model the field. The shell thickness is 0.83-cm; the horizontal edge is 1 cm and the height of the edge is 0.560 m. (The exact minimum is at 0.556.) The feed wire is the same as in the above CST model. The same eigenmode circuit model was used to fit the impedance. The circuit parameters are listed in Table 2**.** In this case, the capacitance and effective height are not known. Alfred R. Lopez [14] published a Q-factor of $Q(ka)^3 = 1.75.$

The same Matlab program was used to numerically fit the data to a two-eigenmode model, Table 2 and Figure 11. Figure 12 shows the magnitude of the error is $< 0.0013\ \Omega$. If the least squares fit was expanded to include the variable C_{OP+}, the error would be smaller. The spherical top load has a larger surface area and a smaller charge density larger than the above antenna. The potential on the spherical top load will be smaller. The DC capacitance is 8% larger than the above antenna. The effective height is 5% smaller than the above antenna. A thinner spherical shell will have less charge on the edge and a higher charge density on the sphere. The higher charge density increases the potential on the sphere; this decreases the capacitance. Moving the edge charge to a higher position increases the effective height. Stuart [19] pointed out that a thicker shell has a higher Q-factor. The feed-line analysis is the same as above. A 1-m monopole has 9.54-pF capacitance. The feed line would have a capacitance around 5 pF. The CST model is reasonable accurate.

The radiation resistance has two components, ω^2 and ω^4:

$$R_{SP} = s_1(\omega/\omega_r)^2 + s_2(\omega/\omega_r)^4, \tag{40}$$

where ω_r is the angular resonant frequency, $s_1 = 1.960684$ and $s_2 = 0.28059356.$ Figure 13 plots the total radiation resistance, the ω^2 and ω^4 terms. The Q is plotted in Figure 14 and the Q-factor is plotted in Figure 15.

Table 2. Spherical top-load data fit to a two-eigenmode model.

Parameters	Eigenmode 1	Eigenmode 1 & 2
C_{SP}	97.20870562 pF	97.20870562 pF
L_{SP}	1.0303518 μH	1.0303518 μH
$R_{0\ SP}$	4.7281347 KΩ	4.7281347 KΩ
$f_{SP\ RES}$	15.90688 MHz	15.90654 MHz
h_{Eff}	0.6649	0.6649
C_{OP}	N/A	6.4012 pF
$f_{Antires}$	N/A	63.964 MHz
$Q-Factor$	N/A	1.70

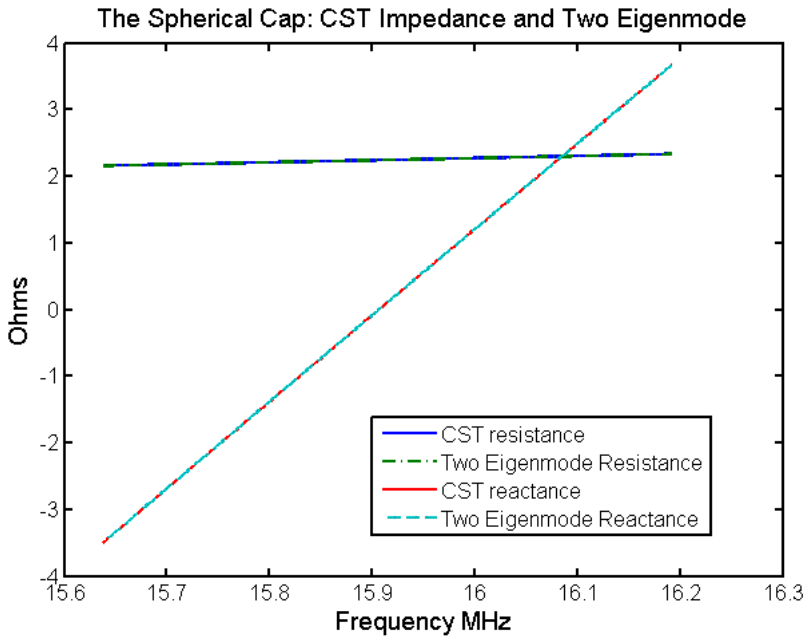

Figure 11. CST impedance and two eigenmode model.

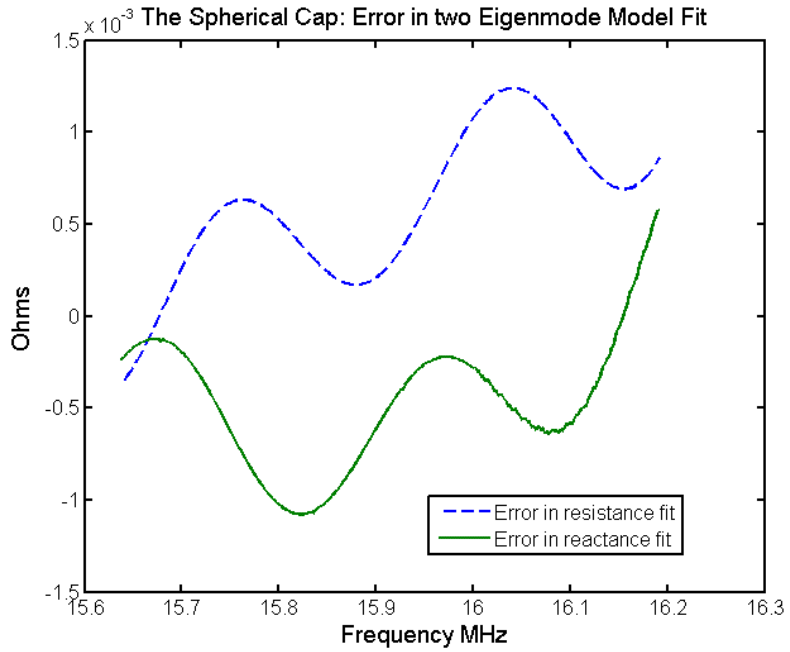

Figure 12. Error in the two-eigenmode model.

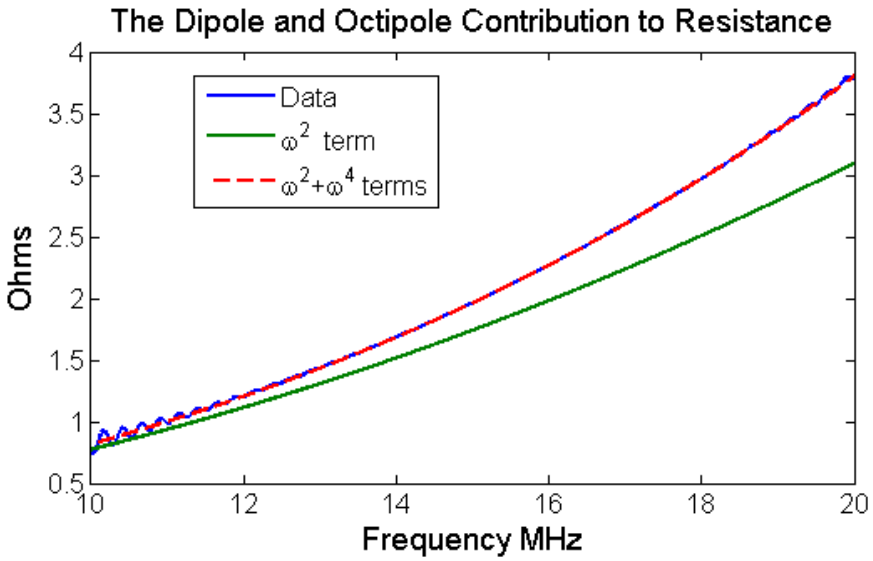

Figure 13. ω^2 and ω^4 components of resistance.

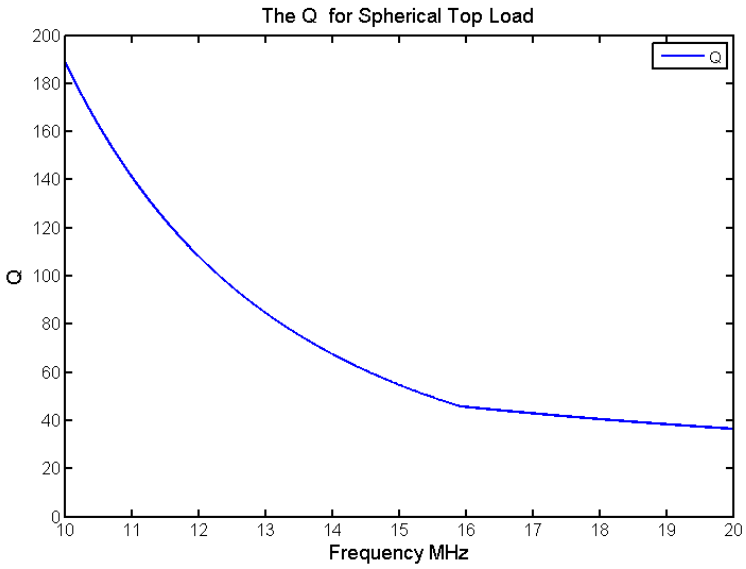

Figure 14. Q for spherical top load.

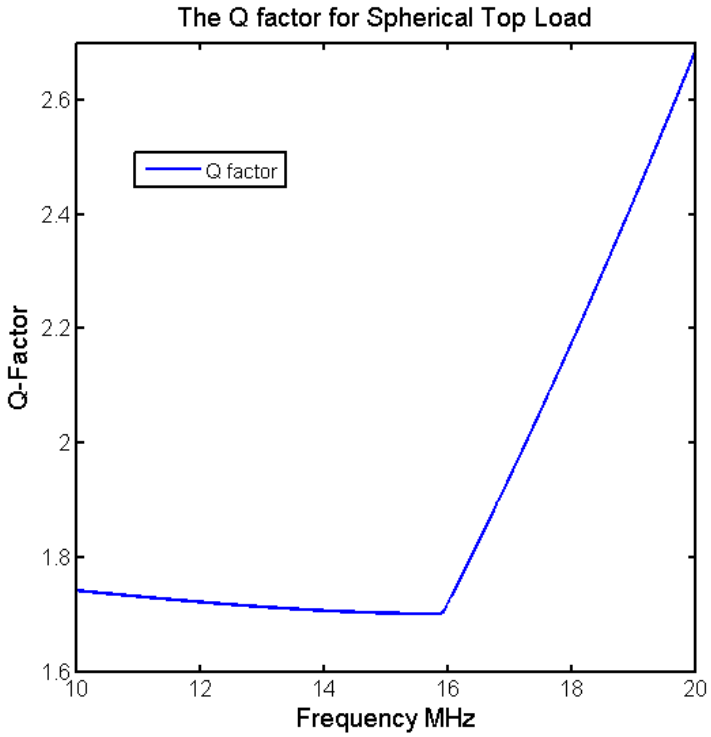

Figure 15. Q-factor for spherical top load.

7. CONCLUSION

The electromagnetic properties of an antenna can be described as a linear combination of eigenmodes. The quasi-static antenna design algorithm is a method for calculating the radiation resistance of the dipole eigenmode (the ω^2 term) and the DC capacitance of the antenna. The three-element circuit model of the dipole eigenmode impedance does not accurately explain the impedance and Q. An accurate model for the impedance requires a contribution from the octupole and higher eigenmodes. The octupole eigenmode can be approximated with a parallel capacitor. The interaction of the dipole and octupole eigenmodes introduces an ω^4 term in the radiation resistance. The octupole eigenmode reduces the antenna Q below the value predicted by the quasi-static antenna design algorithm. The Q limits based optical theorem and a dipole excitation are valid only in the low-frequency limit where the octupole eigenmode does not contribute to the radiation resistance..

The quasi-static antenna design algorithm models a top load as a sum of multipole moments. The algorithm appears to converge in Q and shape. In the case of a spherical enclosure, the Q is only slightly larger than the minimum Q spherical cap monopole. This algorithm allows antennas to be designed with higher radiation resistance and a slightly higher Q [7]. With minor modifications, the same algorithm can be used with different enclosing surfaces.

8. REFERENCES

1. L. J. Chu. 1948. “Physical Limitations of Omnidirectional Antennas,” *Journal of Applied Physics*, vol. 19, no. 12 (December), pp. 1163–1175.

2. H. L. Thal. 2006. “New Radiation Q Limits for Spherical Wire Antennas,” *IEEE Transitions. Antennas and Propagation*, vol. 54, no. 10 (October), pp. 2757–2763.

3. S. R. Best. 2004. “The Radiation Properties of Electrical Small Folder Spherical Helix Antennas,” *IEEE Transactions Antennas and Propagation*, vol. 52 (April), pp. 953–959.

4. M. Gustafsson, C. Sohl, and G. Kristensson. 2009. “Illustrations of New Physical Bounds on Linearly Polarized Antennas,” *IEEE Transactions on Antennas and Propagation*, vol. AP-57, no. 5 (May), pp. 1319–1327.

5. A. D. Yaghjian and H. R. Stuart. 2010. "Lower Bonds on the Q of Electrically Small Dipole Antennas," *IEEE Transactions on Antennas and Propagation*, vol. 58, no. 10 (October).

6. T. O. Jones III. 2012. Quasi-Static Design Approach for Minimizing the Quality Factor ' Q ' for Electrical Small Antennas, U.S. Patent 8,121,821 B1 (February 21).

7. T. O. Jones III. 2011. “A Quasi-Static Antenna Design Approach for Minimum-Q Antennas,” *IEEE Antennas and Propagation Magazine*, vol. 53, no. 3 (June).

8. T. O. Jones III. 2013. Dipole Moment Term for an Electrically Small Antenna, U.S. Patent 8368156 B1 (February 5).

9. S. A. Schelkunoff and H. T. Friis. 1952. *Antennas, Theory and Practice*, pp. 318, Figure 10.9, John Wiley & Sons, Inc., New York, NY.

10. N. C. De, T. K. Ghosh, D. R. Poddar, and S. K. Chowdhury. 1995. “Design and Experimental Investigation of the Asymptotic Conical Dipole Antenna, *IEEE Transactions on Electromagnetic Compatibility*,” vol. 37, no. 2 (May), pp. 282–285.

11. T. Simpson. 2006. “The Scheikunaff-Friis Dipole: the Simplest Antenna of All,” *IEEE Antennas and Propagation Magazine*, vol. 48, no. 4 (August), pp. 48–53.

12. H. D. Foltz, J. S. McLean, and L. Bodner. 2002."Closed-form Lumper Element Model for Folded, Disk Loaded Monopoles." *Proceedings of IEEE Antennas and Propagation Society International Symposium* (pp. 576–579). 16-21 June, San Antonio, TX.

13. H. R. Stuart. 2009. “Eigenmode Analysis of a Two Element Segmented Capped Monopole Antenna,” *IEEE Transactions on Antennas and Propagation*, vol. 57, no. 10 (October), pp. 2980–2888.

14. A. R. Lopez. 2006. “Fundamental Limits of Small Antennas: Validation of Wheeler's Formula,” *IEEE Antenna and Propagation Magazine*, vol. 48, no. 4 (August), pp. 28–35.

15. The author derived this result from [17]; he is not first to calculate this result.

16. I. S. Gradshteyn and I. M. Ryzhik. 1980. *Table of Integrals, Series, and Products*, Corrected and Enlarged Edition, Fourth Edition. Academic Press, New York, NY.

17. G. Arfken. 1970. *Mathematical Methods for Physicists,* Second Edition. Academic Press, New York, NY.

18. A. D. Yaghjian and S. R. Best, Impedance. 2005. “Bandwidth and Q of Antenna,” *IEEE Transactions on Antennas and Propagation*, vol. 53, no. 4 (April), pp. 1298–1324.

19. H. R. Stuart and A. D. Yaghjian. 2010. "Approaching the Lower Bounds on Q for Electrically Small Electric-Dipole Antennas Using High Permeability Shells,” *IEEE Transactions on Antennas and Propagation*, vol. 58, no. 12 (December), pp. 3865–3872.

REPORT DOCUMENTATION PAGE

Form Approved
OMB No. 0704-01-0188

PLEASE DO NOT RETURN YOUR FORM TO THE ABOVE ADDRESS.

1. REPORT DATE *(DD-MM-YYYY)*	2. REPORT TYPE	3. DATES COVERED *(From - To)*
April 2013	Final	

4. TITLE AND SUBTITLE

Convergence of the Quasi-static Antenna Design Algorithm

5a. CONTRACT NUMBER

5b. GRANT NUMBER

5c. PROGRAM ELEMENT NUMBER

6. AUTHORS

T. O. Jones III

5d. PROJECT NUMBER

5e. TASK NUMBER

5f. WORK UNIT NUMBER

7. PERFORMING ORGANIZATION NAME(S) AND ADDRESS(ES)

SSC Pacific
5622 Hull Street
San Diego, CA 92152–5001

8. PERFORMING ORGANIZATION REPORT NUMBER

TR 2016

9. SPONSORING/MONITORING AGENCY NAME(S) AND ADDRESS(ES)

None

10. SPONSOR/MONITOR'S ACRONYM(S)

11. SPONSOR/MONITOR'S REPORT NUMBER(S)

12. DISTRIBUTION/AVAILABILITY STATEMENT

Approved for public release.

13. SUPPLEMENTARY NOTES

14. ABSTRACT

The quasi-static antenna-design algorithm uses multipole basis function to model the general thick top load. A sequence of solutions converge in shape and Q. The absolute minimum Q-factor, 1.825, is obtained for a thick disk top load enclosed by a sphere. This is significantly smaller than the thin disk top load Q-factor 2.349 and previously derived thick-disk Q-factor 2.078. An analytic potential is derived for each multipole basis function. The capacitance and effective height is calculated from the potentials on the enclosing sphere. The impedance is computed with Computer Simulation Technology (CST) Microwave Studio. The impedance data is numerically fit to a dipole eigenmode equivalent circuit. The radiation resistance does not fit the expected ω^2 frequency dependence (effective height).

The error is an ω^4 term that is explained by a capacitor approximated for the octupole eigenmode equivalent circuit. The quasi-static antenna design algorithm predicts the DC capacitance and the dipole eigenmode effective height. The octupole eigenmode increases the radiation resistance. The Q-factor, 1.77, is lower than expected. These results are compared to the spherical cap top load. The existence of an ω^4 limits the accuracy of the theoretical limits in the Q values for antennas.

15. SUBJECT TERMS

oblate speroidal antenna	Q-factor	multipole basis function
radiation resistance	quasi-static antenna	equivalent circuit model
top load	dipole eigenmode	two-eigenode circuit model

16. SECURITY CLASSIFICATION OF:			17. LIMITATION OF ABSTRACT	18. NUMBER OF PAGES	19a. NAME OF RESPONSIBLE PERSON
a. REPORT	b. ABSTRACT	c. THIS PAGE			T. O. Jones III
U	U	U	U	36	19B. TELEPHONE NUMBER *(Include area code)* (619) 553-7082

INITIAL DISTRIBUTION

84300	Library	(2)
85300	Archive/Stock	(1)
52260	T. O. Jones III	(1)

Defense Technical Information Center
Fort Belvoir, VA 22060–6218 (1)

Approved for public release.

SSC Pacific
San Diego, CA 92152-5001